Data Repository for

Substrate controls on valley formation by groundwater on Earth and Mars

Mathieu G. A. Lapotre* **and Michael P. Lamb**
Division of Geological and Planetary Sciences, California Institute of Technology, 1200 E California Boulevard, Pasadena, California 91125, USA

*Current address: Department of Earth and Planetary Sciences, Harvard University, 24 Oxford Street, Cambridge, Massachusetts 02138, USA

SUPPLEMENTAL TEXT

Seepage-erosion Efficiency

Combining momentum conservation ($\tau_b = \rho g h_\mathrm{n} S_\mathrm{b}$, with τ_b the fluid stress at the bed, ρ the fluid density, g the acceleration of gravity, and S_b the bed slope within the valley) and a bed-friction law ($\tau_\mathrm{b} = \rho C_\mathrm{f} \left(\frac{q_0}{h_\mathrm{n}} \right)^2$, with C_f a dimensionless bed-friction factor, and q_0 the fluid discharge per unit width) yields, for steady uniform flow depth within the valley (h_n),

$$h_\mathrm{n} = \left(\frac{C_\mathrm{f} q_0^2}{g S_\mathrm{b}} \right)^{1/3}. \text{ (DR1)}$$

Under the assumption of steady uniform flow within the valley, the critical flow depth for incipient motion of the sediment is

$$h_\mathrm{im} = \frac{\tau_{*\mathrm{c}} R D}{S_\mathrm{b}}, \text{ (DR2)}$$

where D is grain diameter, $R = \frac{(\rho_\mathrm{s} - \rho)}{\rho}$ is submerged specific density of the sediment (with ρ_s and ρ the sediment and water densities, respectively), and $\tau_{*\mathrm{c}}$ is the critical Shields stress for incipient motion of the sediment (which is a function of $\mathrm{Re}_\mathrm{p} = \frac{\sqrt{RgD}D}{\nu}$) (Parker et al., 2003). Combining Equations DR1 and DR2 yields the seepage-erosion efficiency factor,

$$f = \frac{h_\mathrm{n}}{h_\mathrm{im}} = \left(\frac{C_\mathrm{f}}{g} \right)^{1/3} \frac{\left(q_0 S_\mathrm{b} \right)^{2/3}}{\tau_{*\mathrm{c}} R D}. \text{ (DR3)}$$

From Darcy's law, and assuming mass conservation at the seepage face,

$$q_0 = \frac{g \kappa_\mathrm{eff}}{\nu} h \frac{dh}{dx}, \text{ (DR4)}$$

where g is gravitational acceleration, κ_eff is effective aquifer permeability, ν is kinematic viscosity of water, and h is the height of the water table above a horizontal datum leveled with

the bottom of the seepage-erosion face (Fig. 2). Combined with the boundary condition $h(x=0)=h_0$, Equation DR4 yields

$$h(x)=\sqrt{\frac{2q_0\nu}{g\kappa_{\text{eff}}}x+h_0^2}\ . \text{(DR5)}$$

From the considered valley geometry (Fig. 2), it can be seen that another boundary condition is $h(x=L)=H_c+SL$ (with H_c the height of the seepage face, S the topographic slope upstream of the seepage face, and L the drainage-basin length), such that the Darcy discharge per unit width can be rewritten as a function of valley geometry as

$$q_0=\frac{g\kappa_{\text{eff}}}{2L\nu}\left\{\left(H_c+SL\right)^2-h_0^2\right\}. \text{(DR6)}$$

From mass conservation at the seepage face,

$$\phi h_0=h_n, \text{(DR7)}$$

where ϕ is the porosity of the aquifer. Combining Equations 1, DR2, and DR7, one finds that $h_0=\frac{\tau_{*c}RD}{S_b\phi}f$. Finally, substituting for h_0 into Equation DR6, and for q_0 from Equation DR6 into Equation DR3 yields

$$f^{3/2}=\frac{1}{2}\left(\frac{C_f}{g}\right)^{1/2}\frac{g\kappa_{\text{eff}}}{\nu D^{1/2}}\frac{H^*}{L^*}\frac{S_b}{\left(\tau_{*c}R\right)^{3/2}}\left[\left(1+SL^*\right)^2-\left(\frac{\tau_{*c}R}{\phi S_b H^*}\right)^2 f^2\right], \text{(DR8)}$$

which, using the definitions of Da and Re_p can be rewritten as Equation 2.

Because bed-friction coefficient varies with grain size, it can conveniently be parameterized as a function of grain size. We first parameterize the bed-friction coefficient as a function of bed roughness, k, and normal-flow depth, h_n, through (Brownlie, 1983)

$$C_f=\frac{1}{(8.1)^2}\left(\frac{k}{h_n}\right)^{1/3}. \text{(DR9)}$$

Combining Equations 1 and DR2, we can substitute for h_n into Equation DR9,

$$C_f=\frac{1}{65.6}\left(\frac{kS_b}{f\tau_{*c}RD}\right)^{1/3}. \text{(DR10)}$$

We then parameterize the effect of channel-form roughness and grain-size on bed roughness through

$$k=\begin{cases}k_0, & \text{for } D<D_0\\ \alpha D, & \text{for } D\geq D_0\end{cases}, \text{(DR11)}$$

where $k_0\approx 1.7$ cm corresponds to a smooth sand-bedded terrestrial channel (Manning's n value of 0.02) (Chow, 1959), and α is a constant equal to 2.5 (Kamphuis, 1974; Brownlie, 1983). To ensure continuity of roughness as a function of grain size, the cross-over grain size, D_0, is defined as the grain size for which both formulations of k are equal (i.e., $D_0\approx 6.8$ mm).

Permeability

Not all combinations of grain size and permeability are found in natural granular materials; we thus use measurements of naturally occurring gran size and permeability combinations to further constrain the feasibility of seepage erosion in natural substrates.

We first use empirical fits to hydraulic conductivity on consolidated and loose well sorted sediment (Shepherd, 1989) as conservative lower and upper bounds, and thus calculate conservative bounds on intrinsic permeability, κ,

$$\kappa_{\min} = 11.9\left(\frac{\nu}{g}\right)D^{1.5} \text{ (DR12)}$$

and

$$\kappa_{\max} = 6695\left(\frac{\nu}{g}\right)D^{1.85}. \text{ (DR13)}$$

Then, in order to incorporate fluid inertia at high flow rates, we use an apparent permeability (Bear, 1972; Barree and Conway, 2004),

$$\kappa_{\text{eff}} = \frac{\kappa}{1+\text{Re}_{\beta}}, \text{ (DR14)}$$

where $\text{Re}_{\beta} = \frac{u(\beta\kappa)}{\nu}$, with u the water discharge per unit area, and β the Forchheimer coefficient (or inertial factor). It was shown experimentally (Barree and Conway, 2004) that $(\beta\kappa) \approx 2D$ for unconsolidated material. We assume that the latter relation holds for weakly consolidated sediment. Under the assumption of steady uniform flow,

$$\tau_* = \frac{u_*^2}{RgD} = \frac{h_{\text{n}}S_{\text{b}}}{RD}, \text{ (DR15)}$$

where u_* is the flow shear velocity in the valley, and is defined as $\sqrt{\frac{\tau_b}{\rho}}$ with τ_b the boundary shear stress imparted by flow on the valley bed, such that

$$f = \frac{\tau_*}{\tau_{*\text{c}}}. \text{ (DR16)}$$

Using mass conservation, $u \sim \phi u_*$, and combining Equations DR14-DR16, we find that

$$\kappa_{\text{eff}} = \frac{\kappa}{\left(1+2\phi\sqrt{f\tau_{*\text{c}}}\,\text{Re}_{\text{p}}\right)}, \text{ (DR17)}$$

where κ is bounded by $\kappa_{\min}$ and $\kappa_{\max}$ (blue-to-red shaded areas in Figures 3A and DR1-DR6). At low water discharges, $\kappa_{\text{eff}} = \kappa$, and κ_{eff} deviates from κ as water discharge increases due to inertial effects, which causes the permeability to plateau for larger grain sizes.

Why is our model conservative?

Our formulation for the seepage-erosion efficiency factor is conservative because:

- It neglects inertial effects at high groundwater discharges; solving for the full Forcheimer equation, for example, would yield lower seepage discharges for a given permeability, effectively shifting the $f = 1$ boundary to lower grain sizes.
- We assume that all of the groundwater is transmitted to the valley through the seepage face, i.e., that no groundwater discharge is lost to seepage underneath the valley bottom.
- We assume that erosion is transport-limited while in reality seepage discharge may not be sufficient to weather rock and surpass any relevant detachment threshold.
- We solved for the onset of sediment transport ($f = 1$). However, because sediment transport rates are very low at or near the threshold, f needs to be greater than unity for sediment to be removed from the valley head. Solving Equation 2 for $f > 1$ shifts the f boundary to higher permeabilities and the $\kappa_{\text{eff}}(D)$ field to lower permeabilities (Fig. DR1).
- Because we assume detached-sediment sizes are representative of the grain sizes in the aquifer rocks, our model implicitly neglects weathering. The martian valleys we have analyzed appear to be carved into competent basaltic bedrock, as suggested by near-vertical walls, cooling joints, and large boulders that line talus slopes, further suggesting that the rock has not been reduced to sand despite the potential for billions of years of weathering. Weathering could make seepage erosion in rock more likely (e.g., Luo and Howard, 2008), but only if it transforms the rock into a substrate with permeability and erodibility characteristics similar to loose sand, which we find unlikely for basalt. On Earth, basalt, owing to its fine-grained matrix, tends to weather into cohesive clays, not loose sand, by chemical processes in the presence of water. Furthermore, chemical weathering rates of basalt are low, especially at the low temperatures thought to be relevant to Hesperian Mars (Hausrath et al., 2008; Bishop et al., 2018). Freeze-thaw exploits pre-existing weaknesses in the rock fabric, which in basaltic flows mainly consist of flow boundaries and sub-vertical cooling joints. Thus, freeze-thaw would primarily shatter basalt into boulders, whereas any smaller shattered material would fill in the fractures, decreasing the horizontal permeability of weathered rock. Furthermore, freeze-thaw is only effective when temperature oscillates within a narrow range and for slow cooling rates (Walder and Hallet, 1985), conditions that are unlikely representative of diurnal and seasonal temperature variations on Hesperian Mars. Eolian particle impacts can abrade basaltic bedrock, but this is a slow mechanism, it produces fine dust (Sharp, 1964), and it is unclear why it would be focused at spring heads to drive valley formation. Salt weathering would require an unlikely succession and repetition of events: (i) episodic low-discharge briny flows that evaporate at the seepage face, and thus do not transport sediment, in order to precipitate salts in bedrock fractures, (ii) disaggregation of bedrock by salt growth into sand-sized particles during relatively long-lived arid conditions, and (iii) freshwater seepage flows that dissolve salt cements to increase aquifer permeability and achieve higher discharges necessary to transport sediment away from the seepage face and evacuate sediment through valleys tens to hundreds of kilometers in length.

Sensitivity analysis

Although our model formulation is one-dimensional, it is possible that curvature of the valley head causes flow focusing, locally enhancing groundwater discharge. We thus evaluate the effect of three-dimensional groundwater flow by way of a focusing factor, ω, defined as the ratio of actual (q) to one-dimensional (q_0) seepage discharge, such that Equation DR6 is replaced with

$$q = \frac{\omega g \kappa_{\text{eff}}}{2L\nu}\left\{\left(H_{\text{c}} + SL\right)^2 - h_0^2\right\}. \quad \text{(DR18)}$$

In the case of the valleys in the Florida Panhandle, the maximum value of ω was found to be $\omega \approx 5$ by comparing highly curved valley heads and linear escarpments (no curvature) (Petroff et al., 2011). Using $\omega = 5$, we find that seepage erosion remains confined to grain sizes finer than fine gravel in loose sediment and sand-sized, weakly consolidated sedimentary rocks. Even for an unrealistically large value of $\omega = 20$, we find that seepage erosion is not permitted for grain sizes coarser than ~1.5 cm and sand sizes for weakly consolidated sediments (Fig. DR2).

We also evaluate the effect of varying valley depth by a factor of three (H_{c}; Fig. DR3), drainage-basin length by a factor of 100 (L; Fig. DR4), and upstream and downstream bed slopes by a factor of five (S and S_{b}; Figs. DR5 and DR6, respectively). We find that in all of these cases, seepage erosion is only permitted in grain sizes between silt and medium gravel in loose sediment, and in sand sizes for weakly consolidated sediments.

Parameters compilation for case studies

Table DR1 summarizes input parameters. Data from physical experiments comes from previous studies (Howard and McLane, 1988; Lobkovsky et al., 2004; Schorghofer et al., 2004; Lobkovsky et al., 2007). Basin length was measured from 90-m Shuttle Radar Topography Mission (Farr et al., 2007) topography for terrestrial valleys, and Mars Orbiter Laser Altimeter (Smith et al., 2001) topography for martian valleys. Valley depth, and upstream and bottom slopes were measured from Advanced Spaceborne Thermal Emission and Reflection Radiometer (Yamaguchi et al., 1998) and Mars Reconnaissance Orbiter Context Camera (Malin et al., 2007) digital elevation models on Earth and Mars, respectively. Grain size and permeability ranges were compiled from previous studies (Laity and Malin, 1985; Shipton et al., 2002; Lamb et al., 2008; Abrams et al., 2009; Petroff et al., 2011; Lamb et al., 2014; Zuluaga et al., 2014; Lapotre et al., 2016), with the exception of Echus Chasma, for which we used a broad permeability range encompassing fractured rock and estimates for a martian impact megabreccia (Clifford, 1993).

Submerged specific density of sediment is R=1.65 for sediments and sedimentary rocks, and 1.9 for basalt on Earth and Mars. Acceleration of gravity is 9.81 m/s^2 on Earth and 3.71 m/s^2 on Mars. Aquifer porosity is assumed to be 35%, and kinematic viscosity of water is 1×10^{-6} m^2/s.

Data

Topographic data are available at U.S. Geological Survey Earth Resources Observation and Science Center, https://eros.usgs.gov/usa, and Earth Explorer, https://earthexplorer.usgs.gov/, for Earth, and the Planetary Data System, https://pds.nasa.gov/ for Mars.

SUPPLEMENTARY TABLE AND FIGURES

	Used to calculate seepage erosion-efficiency factor, f				Additional constraints	
	Basin length, L (m)	**Seepage-face height, H_c (m)**	**Upstream slope, S**	**Bottom slope, S_b**	**Grain diameter, D (m)**	**Permeability, κ_{eff} (cm^2)**
Sandbox experiments	2	1×10^{-2}	1×10^{-1}	1.5×10^{-1}	3.7×10^{-4} - 7.5×10^{-4}	1.3×10^{-6} - 3×10^{-6}
Florida	1×10^{4}	50	3×10^{-3}	1×10^{-2}	2.8×10^{-4} - 1×10^{-3}	3×10^{-7} - 1.2×10^{-6}
Colorado Plateau	1×10^{4}	100	3×10^{-2}	5×10^{-2}	1.25×10^{-4} - 5×10^{-4}	1×10^{-10} - 5×10^{-9}
Idaho & Washington	4.5×10^{5}	100	3×10^{-3}	1×10^{-2}	0.2-0.7	5.1×10^{-6} - 1×10^{-5}
Echus Chasma, Mars	3×10^{5}	440	3×10^{-3}	1×10^{-2}	1-10	1.0×10^{-11} – 1.0×10^{-4}

Table DR1. Model input parameters. Model input parameters are representative of (i) materials and scales of physical experiments in sand (Howard and McLane, 1988; Lobkovsky et al., 2004; Lobkovsky et al., 2007; Schorghofer et al., 2004), (ii) measurements from orbital imagery and field observations for terrestrial valleys (Abrams et al., 2009; Laity and Malin, 1985; Lamb et al., 2008; Lamb et al., 2014; Lapotre et al., 2016; Petroff et al., 2011; Shipton et al., 2002; Zuluaga et al., 2014), and (iii) measurements from orbital imagery (Lapotre et al., 2016) and a broad permeability range based on lithology for martian valleys and encompassing the case for highly permeable martian megabreccia (Clifford, 1993). Parameters were chosen conservatively as described in the Supplemental Text. Permeability range for the Colorado Plateau valleys is large due to significant spatial and across-scale variability of the Navajo sandstone; however, a true upper bound on effective permeability is likely lower due to compression bands and permeability barriers at the outcrop scale (Shipton et al., 2002; Zuluaga et al., 2014).

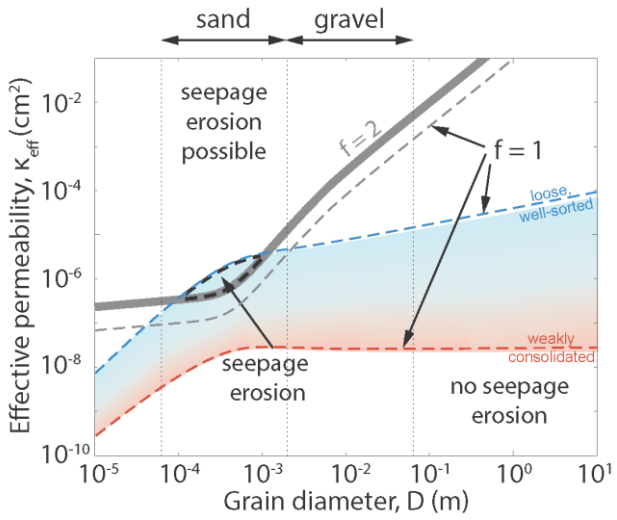

Figure DR1: The case of $f = 2$ for unconsolidated sediment. Input parameters used are those of the Florida Panhandle (Table DR1).

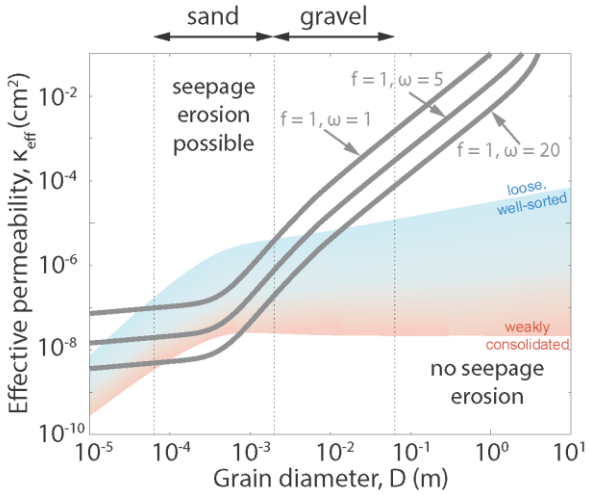

Figure DR2: Effect of focusing of groundwater in the valley head (ω). Input parameters used are those of the Florida Panhandle (Table DR1).

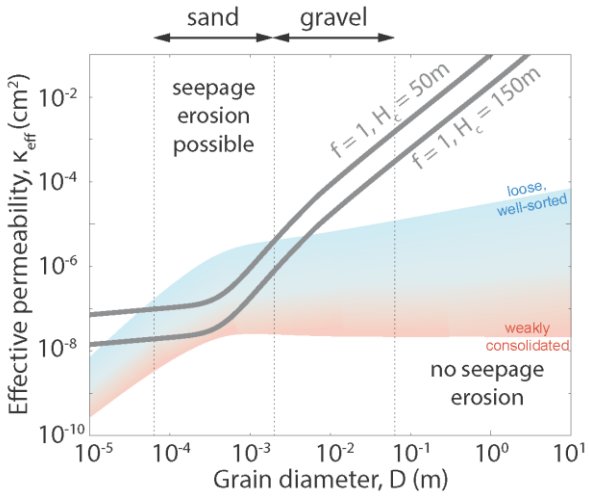

Figure DR3: Effect of varying valley depth (H_c). Other input parameter values are $L = 10$ km, $S = 3\times10^{-3}$, and $S_b = 1\times10^{-2}$.

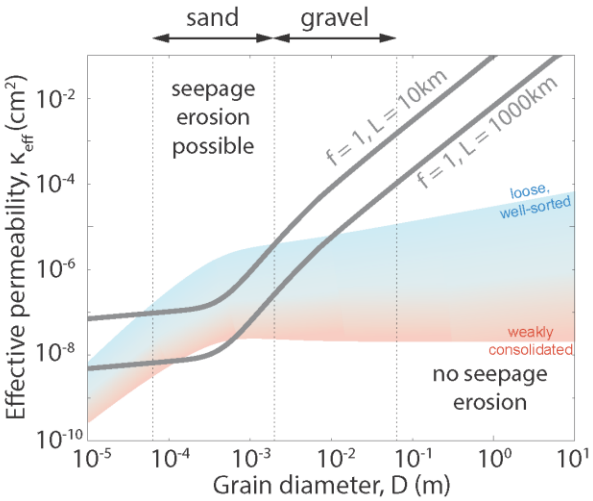

Figure DR4: Effect of varying drainage-basin length (L). Other input parameter values are $H_c = 50$ m, $S = 3\times10^{-3}$, and $S_b = 1\times10^{-2}$.

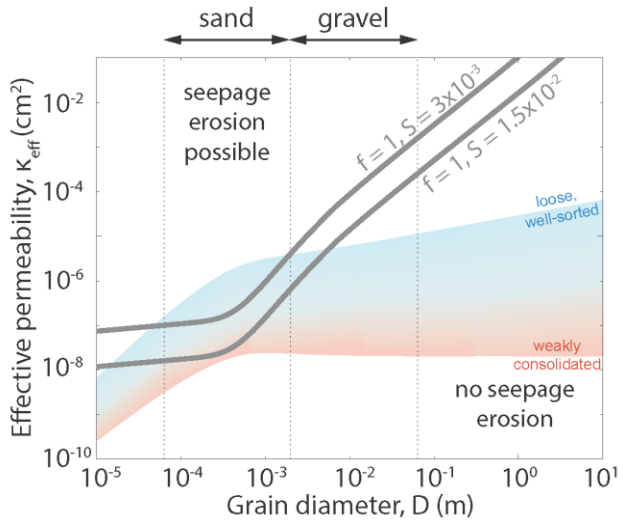

Figure DR5: Effect of varying upstream bed slope (S). Other input parameter values are $H_c = 50\,\text{m}$, $L = 10\,\text{km}$, and $S_b = 1\times10^{-2}$.

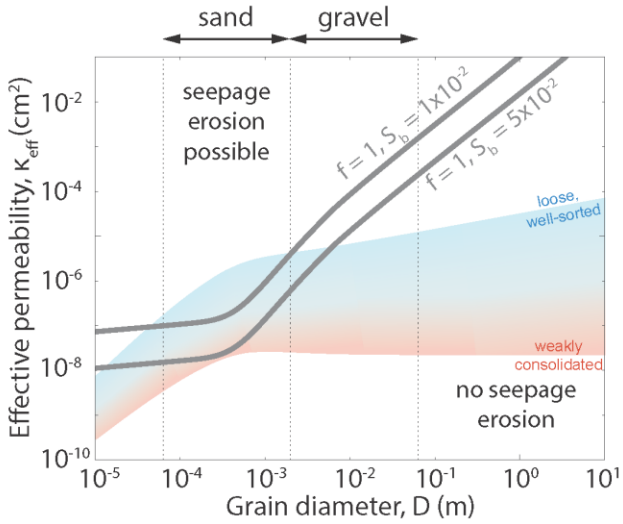

Figure DR6: Effect of varying downstream bed slope (S_b). Other input parameter values are $H_c = 50\,\text{m}$, $L = 10\,\text{km}$, and $S = 3\times10^{-3}$.

REFERENCES CITED

Abrams, D. M., Lobkovsky, A. E., Petroff, A. P., Straub, K. M., McElroy, B., Mohrig, D. C., Kudrolli, A., and Rothman, D. H., 2009, Growth laws for channel networks incised by groundwater flow: Nature Geoscience, v. 2, no. 3, p. 193-196.

Barree, R., and Conway, M., Beyond beta factors: a complete model for Darcy, Forchheimer, and trans-Forchheimer flow in porous media, *in* Proceedings SPE annual technical conference and exhibition2004, Society of Petroleum Engineers.

Bear, J., 1972, Dynamics of flow in porous media, New York, 764 p.

Bishop, J.L., Fairén, A.G., Michalski, J.R., Gago-Duport, L., Baker, L.L., Velbel, M.A., Gross, C., and Rampe, E.B., 2018, Surface clay formation during short-term warmer and wetter conditions on a largely cold ancient Mars: Nature Astronomy, v. 1, https://doi.org/10.1038/s41550-017-0377-9.

Brownlie, W. R., 1983, Flow depth in sand-bed channels: Journal of Hydraulic Engineering, v. 109, no. 7, p. 959-990.

Chow, V., 1959, Open channel hydraulics, New York, McGraw-Hill Book Company, Inc.

Clifford, S.M., 1993, A model for the hydrologic and climatic behavior of water on Mars: Journal of Geophysical Research, v. 98 (E6), p 10,973-11,016, https://doi.org/10.1029/93JE00225.

Farr, T. G., Rosen, P. A., Caro, E., Crippen, R., Duren, R., Hensley, S., Kobrick, M., Paller, M., Rodriguez, E., and Roth, L., 2007, The shuttle radar topography mission: Reviews of Geophysics, v. 45, no. 2.

Hausrath, E.M., Navarre-Sitchler, A.K., Sak, P.B, Steefel, C.I., and Brantley, S.L., 2008, Basalt weathering rates on Earth and the duration of liquid water on the plains of Gusev Crater, Mars: Geology, v. 36 (1), p 67-70, https://doi.org/10.1130/G24238A.1.

Howard, A. D., and McLane, C. F., 1988, Erosion of cohesionless sediment by groundwater seepage: Water Resources Research, v. 24, no. 10, p. 1659-1674.

Kamphuis, J., 1974, Determination of sand roughness for fixed beds: Journal of Hydraulic Research, v. 12, no. 2, p. 193-203.

Laity, J. E., and Malin, M. C., 1985, Sapping processes and the development of theater-headed valley networks on the Colorado Plateau: Geological Society of America Bulletin, v. 96, no. 2, p. 203-217.

Lamb, M. P., Dietrich, W. E., Aciego, S. M., DePaolo, D. J., and Manga, M., 2008, Formation of Box Canyon, Idaho, by megaflood: Implications for seepage erosion on Earth and Mars: Science, v. 320, no. 5879, p. 1067-1070.

Lamb, M. P., Mackey, B. H., and Farley, K. A., 2014, Amphitheater-headed canyons formed by megaflooding at Malad Gorge, Idaho: Proceedings of the National Academy of Sciences, v. 111, no. 1, p. 57-62.

Lapotre, M. G., Lamb, M. P., and Williams, R. M., 2016, Canyon formation constraints on the discharge of catastrophic outburst floods of Earth and Mars: Journal of Geophysical Research: Planets, v. 121, no. 7, p. 1232-1263.

Lobkovsky, A. E., Jensen, B., Kudrolli, A., and Rothman, D. H., 2004, Threshold phenomena in erosion driven by subsurface flow: Journal of Geophysical Research: Earth Surface, v. 109, no. F4.

Lobkovsky, A. E., Smith, B. E., Kudrolli, A., Mohrig, D. C., and Rothman, D. H., 2007, Erosive dynamics of channels incised by subsurface water flow: Journal of Geophysical Research: Earth Surface, v. 112, no. F3.

Luo, W., and Howard, A. D., 2008, Computer simulation of the role of groundwater seepage in forming Martian valley networks: Journal of Geophysical Research: Planets, v. 113, no. E5.

Malin, M. C., Bell, J. F., Cantor, B. A., Caplinger, M. A., Calvin, W. M., Clancy, R. T., Edgett, K. S., Edwards, L., Haberle, R. M., and James, P. B., 2007, Context camera investigation on board the Mars Reconnaissance Orbiter: Journal of Geophysical Research: Planets, v. 112, no. E5.

Parker, G., Toro-Escobar, C. M., Ramey, M., and Beck, S., 2003, Effect of floodwater extraction on mountain stream morphology: Journal of Hydraulic Engineering, v. 129, no. 11, p. 885-895.

Petroff, A. P., Devauchelle, O., Abrams, D. M., Lobkovsky, A. E., Kudrolli, A., and Rothman, D. H., 2011, Geometry of valley growth: Journal of Fluid Mechanics, v. 673, p. 245-254.

Sharp, R.P., 1964, Wind-driven sand in Coachella Valley, California: Geological Society of America Bulletin, v. 75 (9), p. 785–804, https://doi.org/10.1130/0016-7606(1964)75[785:WSICVC]2.0.CO;2.

Schorghofer, N., Jensen, B., Kudrolli, A., and Rothman, D. H., 2004, Spontaneous channelization in permeable ground: Theory, experiment, and observation: Journal of Fluid Mechanics, v. 503, p. 357-374.

Shepherd, R. G., 1989, Correlations of permeability and grain size: Ground water, v. 27, no. 5, p. 633-638.

Shipton, Z. K., Evans, J. P., Robeson, K. R., Forster, C. B., and Snelgrove, S., 2002, Structural heterogeneity and permeability in faulted eolian sandstone: Implications for subsurface modeling of faults: AAPG bulletin, v. 86, no. 5, p. 863-883.

Smith, D. E., Zuber, M. T., Frey, H. V., Garvin, J. B., Head, J. W., Muhleman, D. O., Pettengill, G. H., Phillips, R. J., Solomon, S. C., and Zwally, H. J., 2001, Mars Orbiter Laser Altimeter: Experiment summary after the first year of global mapping of Mars: Journal of Geophysical Research: Planets, v. 106, no. E10, p. 23689-23722.

Walder, J., and Hallet, B., 1985, A theoretical model of the fracture of rock during freezing: Geological Society of America Bulletin, v. 96 (3), p 336-346, https://doi.org/10.1130/0016-7606(1985)96<336:ATMOTF>2.0CO;2.

Yamaguchi, Y., Kahle, A. B., Tsu, H., Kawakami, T., and Pniel, M., 1998, Overview of advanced spaceborne thermal emission and reflection radiometer (ASTER): IEEE Transactions on geoscience and remote sensing, v. 36, no. 4, p. 1062-1071.

Zuluaga, L. F., Fossen, H., and Rotevatn, A., 2014, Progressive evolution of deformation band populations during Laramide fault-propagation folding: Navajo Sandstone, San Rafael monocline, Utah, USA: Journal of Structural Geology, v. 68, p. 66-81.